JOURNAL OF THERMOPHYSICS AND HEAT TRANSFER
Vol. 12, No. 3, July–September 1998

Augmented Burnett and Bhatnagar–Gross–Krook–Burnett Equations for Hypersonic Flow

Keon-Young Yun,* Ramesh K. Agarwal,† and Ramesh Balakrishnan‡
Wichita State University, Wichita, Kansas 67206

Two different forms of Burnett equations are studied that have been designated as augmented Burnett equations and Bhatnagar–Gross–Krook–Burnett (BGK–Burnett) equations. The augmented Burnett equations were developed to stabilize the solution of the conventional Burnett equations that were derived from the Boltzmann equation using the second-order Chapman–Enskog expansion. In this formulation, the conventional Burnett equations are augmented by adding ad hoc third-order derivatives to stress and heat transfer terms so that the augmented equations are stable to small wavelength disturbances. The BGK–Burnett equations have been recently derived from the Boltzmann equation using the BGK approximation for the collision integral. These equations have been shown to be entropy consistent and satisfy the Boltzmann H-theorem in contrast to the conventional Burnett equations that violate the second law of thermodynamics. Both sets of Burnett equations are applied to compute a two-dimensional hypersonic flow over a circular cylinder at Knudsen numbers 0.001–0.1. Comparison is made between the augmented and BGK–Burnett equations solutions and with the Navier–Stokes calculations. Comparison of the solutions of the augmented Burnett equations with the Navier–Stokes solutions shows that the difference is significant at high Knudsen number (Kn = 0.1). The solutions from the BGK–Burnett equations compare reasonably well with those from the Navier–Stokes equations and the augmented Burnett equations.

Nomenclature

e_t = total energy
Kn = Knudsen number
M = Mach number
Pr = Prandtl number
p = pressure
$\boldsymbol{q}_i$ = heat flux
R = gas constant
Re = Reynolds number
T = temperature
T_w = wall temperature
t = time
u, v = velocity components in x and y direction
α_i, β_i = coefficients of stress terms in Burnett equations
γ = specific heat ratio
γ_i = coefficients of heat-flux terms in Burnett equations
δ_i = coefficients of stress terms in Navier–Stokes equations
θ_i = coefficients of third-order terms in BGK–Burnett equations
κ = thermal conductivity
μ = coefficient of viscosity
ρ = density
$\boldsymbol{\sigma}_{ij}$ = stress tensor

Introduction

IN one of the first attempts to solve the Burnett equations, Fiscko and Chapman[1] solved the hypersonic shock structure problem for a variety of Mach numbers and concluded that the Burnett equations describe the normal shock structure better than the Navier–Stokes equations at high Mach numbers. However, in the numerical solution, they experienced stability problems on finer grids. The linearized conventional Burnett equations were found to be unstable to small wavelength disturbances. In a subsequent attempt, Zhong[2] stabilized the Burnett equations by adding a few linear third-order terms on an ad hoc basis. This set of equations was termed the augmented Burnett equations. The augmented Burnett equations did not present stability problems when they were applied to the hypersonic shock structure and hypersonic blunt-body problems. However, the augmented Burnett equations were not entirely successful to compute the flowfields for blunt-body wakes and flat-plate boundary layers. Welder et al.[3] and Comeaux et al.[4] noted that the linear stability analysis is not sufficient to explain the instability of the Burnett equations with increasing Knudsen numbers because of many nonlinear terms present in the Burnett equations. It has been shown by Comeaux et al. that the Burnett equations violate the second law of thermodynamics at high Knudsen numbers.

The highly nonlinear nature of the collision integral in the Boltzmann equation can be simplified by representing the collision integral in the Bhatnagar–Gross–Krook (BGK) form. Balakrishnan and Agarwal[5] have formulated a new set of entropy-consistent one-dimensional Burnett equations from the BGK–Boltzmann equation and used the Navier–Stokes equations to approximate the material derivatives in the second-order terms in the Chapman–Enskog expansion. The material derivatives are thus expressed in terms of spatial derivatives using the Navier–Stokes equations. This set of BGK–Burnett equations contains all of the stress and heat-flux terms reported by Fiscko and Chapman[1] and has additional terms that are similar to the super Burnett equation terms. Balakrishnan and Agarwal[5] showed that one-dimensional BGK–Burnett equations are entropy consistent and satisfy the Boltzmann H-theorem at all Knudsen numbers in contrast to the conventional Burnett equations that have been shown[4] to violate the second law of thermodynamics at higher Knudsen numbers. Balakrishnan and Agarwal extended the one-dimensional BGK–Burnett equations to two-dimensional BGK–Burnett equa-

Presented as Paper 97-0980 at the AIAA 35th Aerospace Sciences Meeting, Reno, NV, Jan. 6–9, 1997; received April 30, 1997; revision received Nov. 25, 1997; accepted for publication Jan. 7, 1998.

*Graduate Research Assistant, Aerospace Engineering Department.
†Bloomfield Distinguished Professor and Chair, Aerospace Engineering Department. Fellow AIAA.
‡Graduate Research Assistant, Aerospace Engineering Department.

tions. In this paper, the two-dimensional augmented Burnett equations[2] and the two-dimensional BGK–Burnett equations were employed to compute and compare the shock structure and other flow properties for hypersonic flow over a blunt body at various Knudsen numbers.

Governing Equations

The governing equations for two-dimensional unsteady compressible viscous flow can be written in Cartesian coordinates as

$$\frac{\partial \boldsymbol{Q}}{\partial t} + \frac{\partial \boldsymbol{E}}{\partial x} + \frac{\partial \boldsymbol{E}}{\partial y} = 0 \tag{1}$$

where

$$\boldsymbol{Q} = \begin{bmatrix} \rho \\ \rho u \\ \rho v \\ e_t \end{bmatrix} \tag{2}$$

In Eq. (1), $\boldsymbol{E}$ and $\boldsymbol{F}$ are the flux vectors of the flow variables $\boldsymbol{Q}$ in the x and y directions, respectively. These flux vectors can be written as

$$\begin{aligned} \boldsymbol{E} &= \boldsymbol{E}_I + \boldsymbol{E}_V \\ \boldsymbol{F} &= \boldsymbol{F}_I + \boldsymbol{F}_V \end{aligned} \tag{3}$$

where $\boldsymbol{E}_I$ and $\boldsymbol{F}_I$ are the inviscid-flux terms and $\boldsymbol{E}_V$ and $\boldsymbol{F}_V$ are the viscous-flux terms given as follows:

$$\boldsymbol{E}_I = \begin{bmatrix} \rho u \\ \rho u^2 + p \\ \rho uv \\ (e_t + p)u \end{bmatrix}, \qquad \boldsymbol{E}_V = \begin{bmatrix} 0 \\ \sigma_{11} \\ \sigma_{12} \\ \sigma_{11}u + \sigma_{12}v + q_1 \end{bmatrix} \tag{4}$$

$$\boldsymbol{F}_I = \begin{bmatrix} \rho v \\ \rho uv \\ \rho v^2 + p \\ (e_t + p)v \end{bmatrix}, \qquad \boldsymbol{F}_V = \begin{bmatrix} 0 \\ \sigma_{21} \\ \sigma_{22} \\ \sigma_{21}u + \sigma_{22}v + q_2 \end{bmatrix} \tag{5}$$

The constitutive equations for a gas flow near thermodynamic equilibrium can be derived as approximate solutions of the Boltzmann equation using the Chapman–Enskog expansion.[2] This method yields the general constitutive relations for the stress tensor $\boldsymbol{\sigma}_{ij}$ and heat-flux vector $\boldsymbol{q}_i$ as follows:

$$\begin{aligned} \boldsymbol{\sigma}_{ij} &= \boldsymbol{\sigma}_{ij}^{(0)} + \boldsymbol{\sigma}_{ij}^{(1)} + \boldsymbol{\sigma}_{ij}^{(2)} + \boldsymbol{\sigma}_{ij}^{(3)} + \cdots + \boldsymbol{\sigma}_{ij}^{(n)} + \mathcal{O}(Kn^{n+1}) \\ \boldsymbol{q}_i &= \boldsymbol{q}_i^{(0)} + \boldsymbol{q}_i^{(1)} + \boldsymbol{q}_i^{(2)} + \boldsymbol{q}_i^{(3)} + \cdots + \boldsymbol{q}_i^{(n)} + \mathcal{O}(Kn^{n+1}) \end{aligned} \tag{6}$$

where n represents the order of accuracy with respect to Kn. Kn is defined as

$$Kn = \lambda / L \tag{7}$$

where L is the macroscopic characteristic length, and the mean free path λ is given by

$$\lambda = \frac{16\mu}{5\rho\sqrt{2\pi RT}} \tag{8}$$

In the case of $Kn \approx 0$, only the first terms in Eqs. (6) are important. The zeroth-order approximation ($n = 0$) results in the Euler equations

$$\boldsymbol{\sigma}_{ij}^{(0)} = 0, \qquad \boldsymbol{q}_i^{(0)} = 0 \tag{9}$$

When $Kn < 0.1$, the first two terms in Eqs. (6) become important for the accurate representation of stress and heat transfer properties of the gas flow. This first-order approximation represents the Navier–Stokes equations. The stress tensor and the heat-flux terms ($n = 1$) are given as

Table 1 Coefficients in the Navier–Stokes equation stress tensor for air

	Augmented Burnett equations	BGK–Burnett equations, $\gamma = 1.4$
δ_1	1.333	−1.6
δ_2	−0.666	−0.4

$$\begin{gathered} \sigma_{11}^{(1)} = -\mu(\delta_1 u_x + \delta_2 v_y), \qquad \sigma_{12}^{(1)} = \sigma_{21}^{(1)} = -\mu(u_y + v_x) \\ \sigma_{22}^{(1)} = -\mu(\delta_1 v_y + \delta_2 u_x) \\ q_1^{(1)} = -\kappa T_x, \qquad q_2^{(1)} = -\kappa T_y \end{gathered} \tag{10}$$

where $(\ )_x = \partial/\partial x$ and $(\ )_y = \partial/\partial y$. The coefficients δ_1 and δ_2 are given in Table 1 for the augmented Burnett equations[2] and the BGK–Burnett equations.

As Kn becomes larger (>0.1), additional higher-order terms in Eqs. (6) are required. The second-order approximation yields the Burnett equations that retain the first three terms in Eqs. (6). The expression for stress and heat-flux terms ($n = 2$) are obtained as

$$\begin{aligned} \sigma_{11}^{(2)} = \frac{\mu^2}{p}\Bigg(&\alpha_1 u_x^2 + \alpha_2 u_x v_y + \alpha_3 v_y^2 + \alpha_4 u_y v_x + \alpha_5 u_y^2 \\ &+ \alpha_6 v_x^2 + \alpha_7 RT_{xx} + \alpha_8 RT_{yy} + \alpha_9 \frac{RT}{\rho}\rho_{xx} + \alpha_{10}\frac{RT}{\rho}\rho_{yy} \\ &+ \alpha_{11}\frac{RT}{\rho^2}\rho_x^2 + \alpha_{12}\frac{R}{\rho}T_x\rho_x + \alpha_{13}\frac{R}{T}T_x^2 + \alpha_{14}\frac{RT}{\rho^2}\rho_y^2 \\ &+ \alpha_{15}\frac{R}{\rho}T_y\rho_y + \alpha_{16}\frac{R}{T}T_y^2\Bigg) \end{aligned} \tag{11}$$

$$\begin{aligned} \sigma_{22}^{(2)} = \frac{\mu^2}{p}\Bigg(&\alpha_1 v_y^2 + \alpha_2 u_x v_y + \alpha_3 u_x^2 + \alpha_4 u_y v_x + \alpha_5 v_x^2 \\ &+ \alpha_6 u_y^2 + \alpha_7 RT_{yy} + \alpha_8 RT_{xx} + \alpha_9 \frac{RT}{\rho}\rho_{yy} + \alpha_{10}\frac{RT}{\rho}\rho_{xx} \\ &+ \alpha_{11}\frac{RT}{\rho^2}\rho_y^2 + \alpha_{12}\frac{R}{\rho}T_y\rho_y + \alpha_{13}\frac{R}{T}T_y^2 + \alpha_{14}\frac{RT}{\rho^2}\rho_x^2 \\ &+ \alpha_{15}\frac{R}{\rho}T_x\rho_x + \alpha_{16}\frac{R}{T}T_x^2\Bigg) \end{aligned} \tag{12}$$

$$\begin{aligned} \sigma_{12}^{(2)} &= \sigma_{21}^{(2)} \\ &= \frac{\mu^2}{p}\Bigg(\beta_1 u_x u_y + \beta_2 u_y v_y + \beta_2 u_x v_x + \beta_1 v_1 v_x v_y \\ &\qquad + \beta_3 RT_{xy} + \beta_4 \frac{RT}{\rho}\rho_{xy} + \beta_5 \frac{R}{T}T_x T_y \\ &\qquad + \beta_6 \frac{RT}{\rho^2}\rho_x\rho_y + \beta_7 \frac{R}{\rho}\rho_x T_y + \beta_7 \frac{R}{\rho}T_x\rho_y\Bigg) \end{aligned} \tag{13}$$

$$\begin{aligned} q_1^{(2)} = \frac{\mu^2}{\rho}\Bigg(&\gamma_1 \frac{1}{T}T_x u_x + \gamma_2 \frac{1}{T}T_x v_y + \gamma_3 u_{xx} + \gamma_4 u_{yy} + \gamma_5 v_{xy} \\ &+ \gamma_6 \frac{1}{T}T_y v_x + \gamma_7 \frac{1}{T}T_y u_y + \gamma_8 \frac{1}{\rho}\rho_x u_x + \gamma_9 \frac{1}{\rho}\rho_x v_y \\ &+ \gamma_{10}\frac{1}{\rho}\rho_y u_y + \gamma_{11}\frac{1}{\rho}\rho_y v_x\Bigg) \end{aligned} \tag{14}$$

$$q_2^{(2)} = \frac{\mu^2}{\rho}\left(\gamma_1 \frac{1}{T} T_y v_y + \gamma_2 \frac{1}{T} T_y u_x + \gamma_3 v_{yy} + \gamma_4 v_{xx} + \gamma_5 u_{xy} + \gamma_6 \frac{1}{T} T_x u_y + \gamma_7 \frac{1}{T} T_x v_x + \gamma_8 \frac{1}{\rho} \rho_y v_y + \gamma_9 \frac{1}{\rho} \rho_y u_x + \gamma_{10} \frac{1}{\rho} \rho_x v_x + \gamma_{11} \frac{1}{\rho} \rho_x u_y\right) \tag{15}$$

Both augmented Burnett and BGK–Burnett equations have the same forms of the stress tensor and heat-flux terms in the second-order approximation. However, the two sets of equations have different values of the coefficients. The coefficients are compared in Table 2.

The third-order approximation ($n = 3$) represents the super Burnett equations. However, not all of the third-order terms of the super Burnett equations are used in the augmented Burnett and the BGK–Burnett equations. In the augmented Burnett equations, the third-order terms are added on an ad hoc basis to obtain stable numerical solutions while maintaining second-order accuracy of the solutions. The third-order terms in the augmented Burnett equations[2] are given as

$$\sigma_{11}^{(a)} = \frac{\mu^3}{p^2} RT(\alpha_{17} u_{xxx} + \alpha_{17} u_{xyy} + \alpha_{18} v_{xxy} + \alpha_{18} v_{yyy}) \tag{16}$$

$$\sigma_{22}^{(a)} = \frac{\mu^3}{p^2} RT(\alpha_{17} v_{yyy} + \alpha_{17} v_{xxy} + \alpha_{18} u_{xyy} + \alpha_{18} u_{xxx}) \tag{17}$$

Table 2 Coefficients of the second-order stress and heat-flux terms in the augmented Burnett and BGK–Burnett equations for air

	Augmented Burnett equations, hard-sphere gas	BGK–Burnett equations, $\gamma = 1.4$
α_1	1.199	−2.24
α_2	0.153	−0.48
α_3	−0.600	0.56
α_4	−0.115	−1.20
α_5	1.295	0.0
α_6	−0.733	0.0
α_7	0.260	−19.6
α_8	−0.130	−5.6
α_9	−1.352	−1.6
α_{10}	0.676	0.4
α_{11}	1.352	1.6
α_{12}	−0.898	−19.6
α_{13}	0.600	−18.0
α_{14}	−0.676	−0.4
α_{15}	0.449	−5.6
α_{16}	−0.300	−6.9
β_1	−0.115	−1.4
β_2	1.913	−1.4
β_3	0.390	0.0
β_4	−2.028	−2.0
β_5	−0.900	2.0
β_6	2.028	2.0
β_7	−0.676	0.0
γ_1	10.830	−25.241
γ_2	0.407	−0.2
γ_3	−2.269	−1.071
γ_4	1.209	−2.0
γ_5	−3.478	−2.8
γ_6	−0.611	−7.5
γ_7	11.033	−11.0
γ_8	−2.060	−1.271
γ_9	1.030	1.0
γ_{10}	−1.545	−3.0
γ_{11}	−1.545	−3.0

$$\sigma_{12}^{(a)} = \sigma_{21}^{(a)} = \frac{\mu^3}{p^2} RT(\beta_8 u_{xxy} + \beta_8 u_{yyy} + \beta_8 v_{xyy} + \beta_8 v_{xxx}) \tag{18}$$

$$q_1^{(a)} = \frac{\mu^3}{p\rho} R\left(\gamma_{12} T_{xxx} + \gamma_{12} T_{xyy} + \gamma_{13} \frac{T}{\rho} \rho_{xxx} + \gamma_{13} \frac{T}{\rho} \rho_{xyy}\right) \tag{19}$$

$$q_2^{(a)} = \frac{\mu^3}{p\rho} R\left(\gamma_{12} T_{yyy} + \gamma_{12} T_{xxy} + \gamma_{13} \frac{T}{\rho} \rho_{yyy} + \gamma_{13} \frac{T}{\rho} \rho_{xxy}\right) \tag{20}$$

The superscript (a) denotes the augmented Burnett terms. The coefficients in stress and heat-flux terms are given as follows: α_{17}, 0.2222; α_{18}, −0.1111; β_8, 0.1667; γ_{12}, 0.6875; and γ_{13}, −0.625.

The BGK–Burnett equations have more additional third-order terms than the augmented Burnett equations. These are not added on an ad hoc basis but are derived from the second-order Chapman–Enskog expansion of the BGK–Boltzmann equation. The third-order terms in the BGK–Burnett equations are given as

$$\begin{aligned}\sigma_{11}^{(B)} = {}& \frac{\mu^3}{p^2} RT(\theta_1 u_{xxx} + \theta_2 u_{xyy} + \theta_3 v_{xxy} + \theta_4 v_{yyy}) \\ & - \frac{\mu^3}{p^2}\frac{RT}{\rho}(\theta_1 \rho_x u_{xx} + \theta_5 \rho_x v_{xy} + \theta_6 \rho_x u_{yy} + \theta_7 \rho_y v_{xx} \\ & + \theta_8 \rho_y u_{xy} + \theta_4 \rho_y v_{yy}) + \frac{\mu^3}{p^2}(\theta_9 u_x^3 + 3\theta_{10} u_x^2 v_y \\ & + \theta_{11} u_x v_y^2 - \theta_4 u_x u_y^2 - 2\theta_4 u_x u_y v_x - \theta_4 u_x v_x^2 + \theta_{10} v_y^3 \\ & - \theta_{12} v_y u_y^2 - 2\theta_{12} u_y v_x v_y - \theta_{12} v_x^2 v_y) + \frac{\mu^3}{p^2} R(\theta_{13} u_x T_{xx} \\ & + \theta_{13} u_x T_{yy} + \theta_{14} v_y T_{xx} + \theta_{14} v_y T_{yy})\end{aligned} \tag{21}$$

$$\begin{aligned}\sigma_{22}^{(B)} = {}& \frac{\mu^3}{p^2} RT(\theta_1 v_{yyy} + \theta_2 v_{xxy} + \theta_3 u_{xyy} + \theta_4 u_{xxx}) \\ & - \frac{\mu^3}{p^2}\frac{RT}{\rho}(\theta_1 \rho_y v_{yy} + \theta_5 \rho_y u_{xy} + \theta_6 \rho_y v_{xx} + \theta_7 \rho_y u_{yy} + \theta_8 \rho_x v_{xy} \\ & + \theta_4 \rho_x u_{xx}) + \frac{\mu^3}{p^2}(\theta_9 v_y^3 + 3\theta_{10} v_y^2 u_x + \theta_{11} v_y u_x^2 - \theta_4 v_y v_x^2 \\ & - 2\theta_4 v_y v_x u_y - \theta_4 v_y u_y^2 + \theta_{10} u_x^3 - \theta_{12} u_x v_x^2 - 2\theta_{12} v_x u_y u_x \\ & - \theta_{12} u_y^2 u_x) + \frac{\mu^3}{p^2} R(\theta_{13} v_y T_{yy} + \theta_{13} v_y T_{xx} + \theta_{14} u_x T_{yy} \\ & + \theta_{14} u_x T_{xx})\end{aligned} \tag{22}$$

$$\begin{aligned}\sigma_{12}^{(B)} = {}& \frac{\mu^3}{p^2} RT(\theta_{15} u_{xxy} + u_{yyy} + \theta_{15} v_{xyy} + v_{xxx}) \\ & - \frac{\mu^3}{p^2}\frac{RT}{\rho}(\theta_6 \rho_y u_{xx} + \theta_{16} \rho_y v_{xy} + \rho_y u_{yy} + \rho_x v_{xx} + \theta_{16} \rho_x u_{xy} \\ & + \theta_6 \rho_x v_{yy}) - \frac{\mu^3}{p^2}(u_y + v_x)(\theta_4 u_x^2 + 2\theta_{12} u_x v_y + 2\theta_7 u_y v_x \\ & + \theta_7 u_y^2 + \theta_7 v_x^2 + \theta_4 v_y^2) + \frac{\mu^3}{p^2} R(\theta_{17} u_y T_{xx} + \theta_{17} u_y T_{yy} \\ & + \theta_{17} v_x T_{xx} + \theta_{17} v_x T_{yy})\end{aligned} \tag{23}$$

$$
\begin{aligned}
q_1^{(B)} = {} & \frac{\mu^3}{p\rho} R \left(\theta_{18} T_{xxx} + \theta_{18} T_{xyy} - \theta_{18} \frac{1}{\rho} \rho_x T_{xx} \right. \\
& \left. - \theta_{18} \frac{1}{\rho} \rho_x T_{yy} \right) + \frac{\mu^3}{p\rho} (\theta_{19} u_x u_{xx} + \theta_{20} u_x v_{xy} + \theta_6 u_x u_{yy} \\
& + \theta_{21} v_y u_{xx} + \theta_{22} v_y v_{xy} + \theta_7 v_y u_{yy} + \theta_{23} u_y v_{xx} \\
& + \theta_{24} u_y u_{xy} + \theta_6 u_y v_{yy} + \theta_{23} v_x v_{xx} + \theta_{24} v_x u_{xy} + \theta_6 v_x v_{yy}) \\
& - \frac{\mu^3}{p\rho} \left(\frac{1}{\rho} \rho_x + \frac{1}{T} T_x \right) (\theta_{13} u_x^2 + 2\theta_{14} u_x v_y + 2\theta_{17} u_y v_x \\
& + \theta_{17} u_y^2 + \theta_{17} v_x^2 + \theta_{13} v_y^2) + \frac{\mu^3}{p\rho} \frac{R}{T} (\theta_{18} T_x T_{xx} + \theta_{18} T_x T_{yy})
\end{aligned} \tag{24}
$$

$$
\begin{aligned}
q_2^{(B)} = {} & \frac{\mu^3}{p\rho} R \left(\theta_{18} T_{yyy} + \theta_{18} T_{xxy} - \theta_{18} \frac{1}{\rho} \rho_y T_{yy} - \theta_{18} \frac{1}{\rho} \rho_y T_{xx} \right) \\
& + \frac{\mu^3}{p\rho} (\theta_{19} v_y v_{yy} + \theta_{20} v_y u_{xy} + \theta_6 v_y v_{xx} + \theta_{21} u_x v_{yy} \\
& + \theta_{22} u_x u_{xy} + \theta_7 u_x v_{xx} + \theta_{23} v_x u_{yy} + \theta_{24} v_x v_{xy} \\
& + \theta_6 v_x u_{xx} + \theta_{23} u_y u_{yy} + \theta_{24} u_y y_{xy} + \theta_6 u_y u_{xx}) \\
& - \frac{\mu^3}{p\rho} \left(\frac{1}{\rho} \rho_y + \frac{1}{T} T_y \right) (\theta_{13} u_x^2 + 2\theta_{14} u_x v_y + 2\theta_{17} u_y v_x \\
& + \theta_{17} u_y^2 + \theta_{17} v_x^2 + \theta_{13} v_y^2) + \frac{\mu^3}{p\rho} \frac{R}{T} (\theta_{18} T_y T_{xx} + \theta_{18} T_y T_{yy})
\end{aligned} \tag{25}
$$

The superscript (B) denotes third-order stress and heat-flux terms in the BGK–Burnett equations. The θ_i are given as follows: ($\gamma = 1.4$) θ_1, 2.56; θ_2, 1.36; θ_3, 0.56; θ_4, −0.64; θ_5, 0.96; θ_6, 1.6; θ_7, −0.4; θ_8, −0.24; θ_9, 1.024; θ_{10}, −0.256; θ_{11}, 1.152; θ_{12}, 0.16; θ_{13}, 2.24; θ_{14}, −0.56; θ_{15}, 3.6; θ_{16}, 0.6; θ_{17}, 1.4; θ_{18}, 4.9; θ_{19}, 7.04; θ_{20}, −0.16; θ_{21}, −1.76; θ_{22}, 4.24; θ_{23}, 3.8; and θ_{24}, 3.4.

Finally, governing Eqs. (1) are nondimensionalized[6] by a reference length and freestream variables and are written in a curvilinear coordinate system (ξ, η) by employing a coordinate transformation[6]:

$$\tau = t, \qquad \xi = \xi(x, y), \qquad \eta = \eta(x, y) \tag{26}$$

Numerical Method

An explicit finite difference scheme has been employed to solve the governing equations. The Steger–Warming flux-vector splitting method[7] is applied to the inviscid-flux terms. The second-order, central-differencing scheme is applied to the stress tensor and heat-flux terms. In the blunt-body flowfield calculations reported in this paper, freestream conditions were used along the outer boundary. First-order extrapolation of the interior data was used to determine the flow properties along the exit boundary. Symmetry boundary conditions were applied to the stagnation streamline. The first-order Maxwell-Smoluchowski slip boundary conditions[2] were used on the wall surface boundary. The first-order Maxwell-Smoluchowski slip boundary conditions in Cartesian coordinates are

$$u_s = \frac{2 - \bar{\sigma}}{\bar{\sigma}} \, \bar{l} \left(\frac{\partial u}{\partial y} \right)_s + \frac{3}{4} \frac{\mu}{\rho T} \left(\frac{\partial T}{\partial x} \right)_s \tag{27}$$

$$T_s = T_w + \frac{2 - \bar{\alpha}}{\bar{\alpha}} \frac{2\gamma}{\gamma + 1} \frac{\bar{l}}{Pr} \left(\frac{\partial T}{\partial y} \right)_s \tag{28}$$

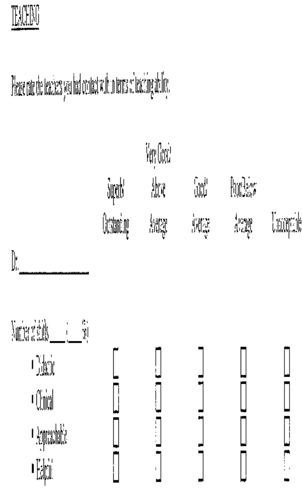

Fig. 1 Computational mesh around a circular cylinder (50 × 82 grid).

where

$$\bar{l} = (2\mu/\rho)\sqrt{\pi/8RT}$$

The subscript s denotes the flow variables on the solid surface of the body. The reflection coefficient $\bar{\sigma}$ and the accommodation coefficient $\bar{\alpha}$ were assumed as 1 (for complete accommodation) in this study.

Application to Blunt Body

The augmented Burnett and the BGK–Burnett equations are applied to compute the hypersonic flow over a cylindrical leading edge with nose radii of 2, 0.2, and 0.02 m. Because the numbers of grid lines are fixed in ξ and η directions, the smaller cylinder has the finer grid system in the physical domain. The grid system in the physical domain is shown in Fig. 1. The flow conditions are

$$M_\infty = 10.0, \qquad Re_\infty = 8396.8/\text{m}, \qquad P_\infty = 2.3881\ \text{N/m}^2$$
$$T_\infty = 208.4\ \text{K}, \qquad T_w = 1000.0\ \text{K}$$

The coefficient of viscosity is calculated by the Sutherland's law

$$\mu = c_1 \frac{T^{3/2}}{T + c_2} \tag{29}$$

Various constants used in the calculation for air are

$$\gamma = 1.4, \qquad Pr = 0.72, \qquad R = 287.04\ \text{m}^2/(\text{s}^2 \cdot \text{K})$$
$$c_1 = 1.458 \times 10^6\ \text{kg/s} \cdot \text{m} \cdot \text{K}^{1/2}, \qquad c_2 = 110.4\ \text{K}$$

With the given flow conditions and constants, the computations were performed at Knudsen numbers of 0.1, 0.01, and 0.001 corresponding to the cylinder radii of 0.02, 0.2, and 2 m, respectively.

Results and Discussion

Case 1: ($Kn = 0.1$)

The comparisons of density and temperature changes along the stagnation streamline are shown in Figs. 2 and 3, respectively. The present augmented and BGK–Burnett solutions are generally consistent with those of Zhong.[2] Also, the present augmented Burnett solutions and BGK-Burnett solutions are almost identical. The temperature curves (Fig. 3) show that the present augmented and BGK–Burnett solutions using the Steger–Warming scheme have a slightly higher maximum temperature than reported by Zhong.[2] The Navier–Stokes solutions are also compared with the augmented and BGK–Burnett solutions in Figs. 2 and 3. Because the flow is in the continuum-transition regime in this case, the differences between the Navier–Stokes and the Burnett solutions are significant. The shock width in both the augmented and BGK–Burnett solutions is larger and the shock is upstream of that in the Navier–Stokes solution. The density and temperature contours of the Navier–Stokes solutions, the augmented Burnett, and BGK–Burnett solutions using the present scheme are shown in Figs. 4–9. The shock structure of the present augmented and BGK–Burnett solutions agrees well with that of Zhong.[2] The BGK–Burnett

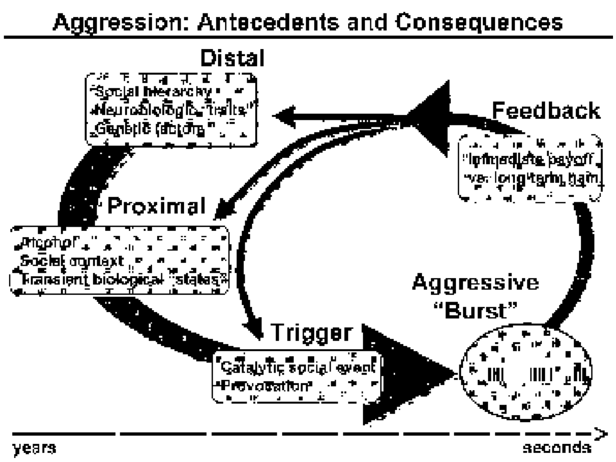

Fig. 2 Density along stagnation streamline for case 1 (Kn = 0.1).

Fig. 3 Temperature along stagnation streamline for case 1 (Kn = 0.1).

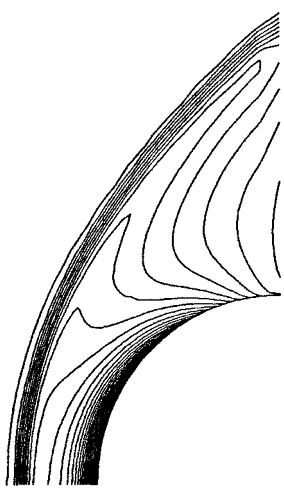

Fig. 4 Navier–Stokes density contours for case 1 (Kn = 0.1).

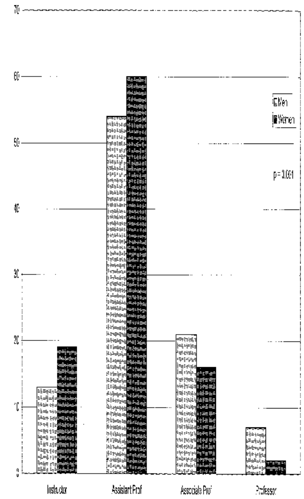

Fig. 5 Augmented Burnett density contours for case 1 (Kn = 0.1).

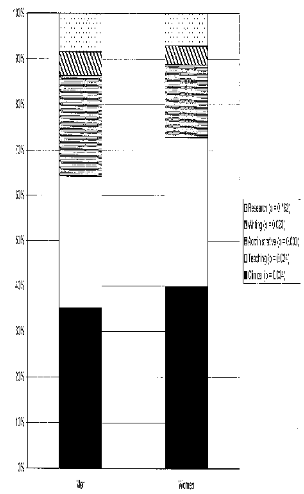

Fig. 6 BGK–Burnett density contours for case 1 (Kn = 0.1).

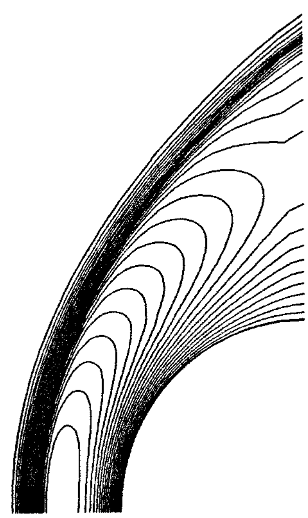

Fig. 7 Navier–Stokes temperature contours for case 1 (Kn = 0.1).

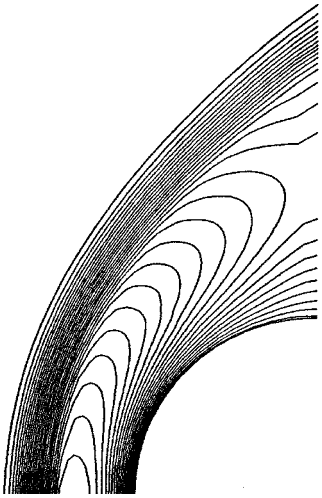

Fig. 8 Augmented Burnett temperature contours for case 1 (*Kn* = 0.1).

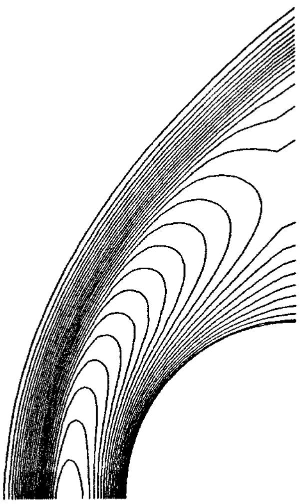

Fig. 9 BGK–Burnett temperature contours for case 1 (*Kn* = 0.1).

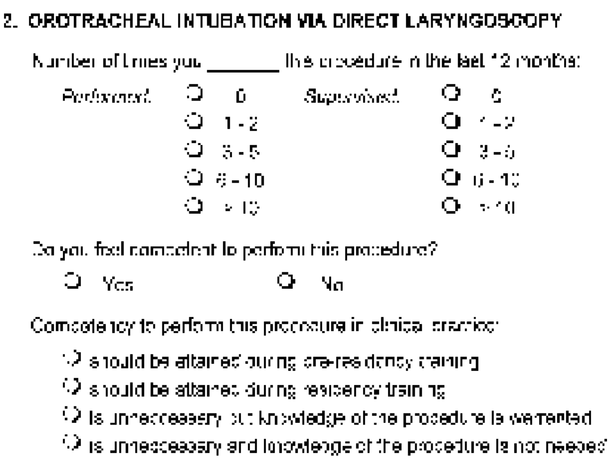

2. OROTRACHEAL INTUBATION VIA DIRECT LARYNGOSCOPY

Number of times you ________ the procedure in the last 12 months:

Performed:	○ 0	Supervised:	○ 0
	○ 1 - 2		○ 1 - 2
	○ 3 - 5		○ 3 - 5
	○ 6 - 10		○ 6 - 10
	○ > 10		○ > 10

Do you feel competent to perform this procedure?

○ Yes ○ No

Competency to perform this procedure in clinical practice:

○ should be attained during pre-residency training
○ should be attained during residency training
○ is unnecessary but knowledge of the procedure is warranted
○ is unnecessary and knowledge of the procedure is not needed

Fig. 10 Density along stagnation streamline for case 2 (*Kn* = 0.01).

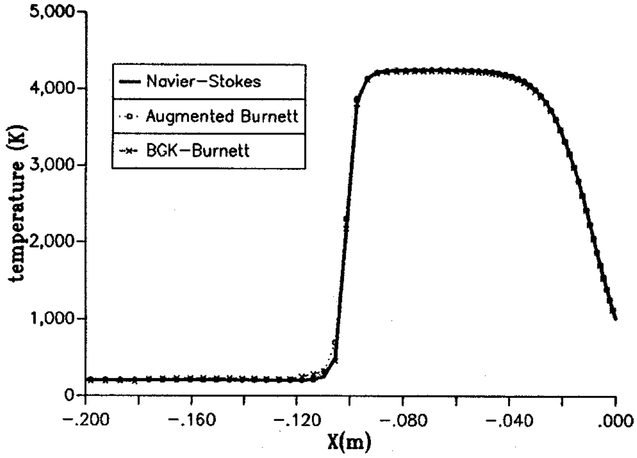

Fig. 11 Temperature along stagnation streamline for case 2 (*Kn* = 0.01).

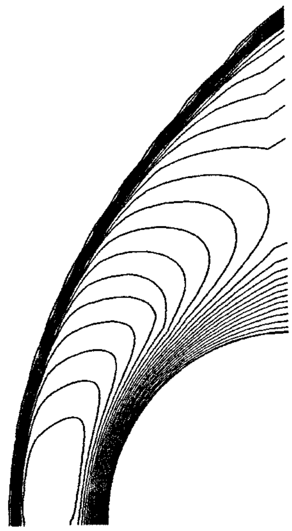

Fig. 12 Navier–Stokes temperature contours for case 2 (*Kn* = 0.01).

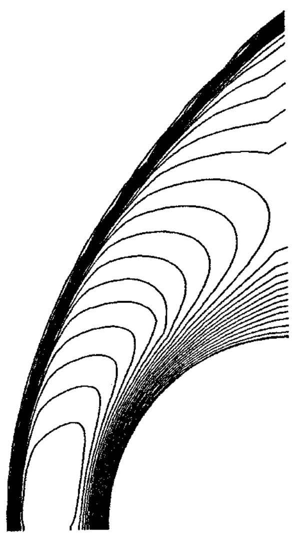

Fig. 13 Augmented Burnett temperature contours for case 2 (*Kn* = 0.01).

solutions are almost identical to the augmented Burnett solutions.

Case 2: (*Kn* = 0.01)

The comparisons of density and temperature changes along the stagnation streamline between the Navier–Stokes, the augmented Burnett, and the BGK–Burnett solutions are shown in Figs. 10 and 11, respectively. The resulting curves are almost coincident with each other. Only small differences are observed at the front of the shock. The temperatue curve of the BGK–Burnett solution (Fig. 11) shows higher temperature than other curves at the front of the shock. The density and temperature contours of each equation solution are also shown in Figs. 12–14. The shock structures are also similar to each other.

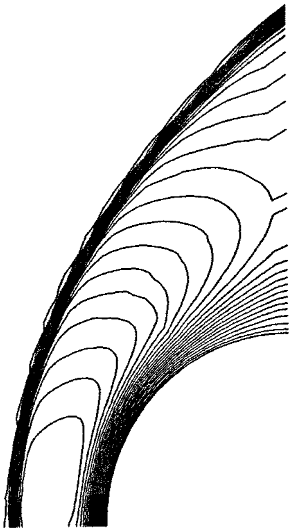

Fig. 14 BGK–Burnett temperature contours for case 2 (Kn = 0.01).

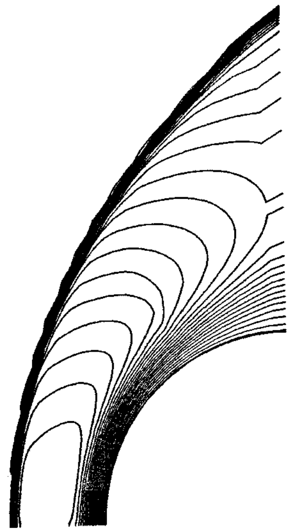

Fig. 17 Augmented Burnett temperature contours for case 3 (Kn = 0.001).

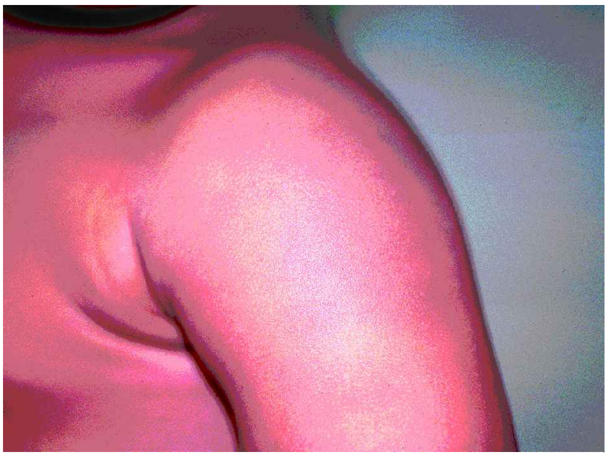

Fig. 15 Density along stagnation streamline for case 3 (Kn = 0.001).

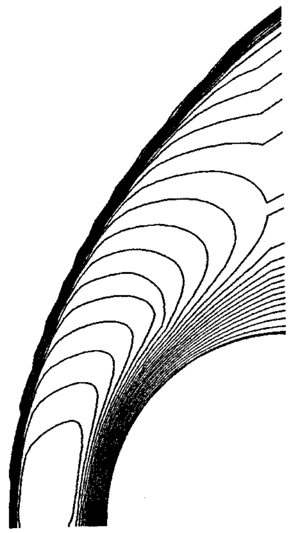

Fig. 18 BGK–Burnett temperature contours for case 3 (Kn = 0.001).

Fig. 16 Temperature along stagnation streamline for case 3 (Kn = 0.001).

Case 3: (Kn = 0.001)

At this small Knudsen number, the solutions of the Navier–Stokes, the augmented Burnett, and the BGK–Burnett equations are identical. Because the flow is in the continuum regime, the Navier–Stokes equations already describe the flowfield accurately. Figures 15 and 16 show the density and temperature changes along the stagnation streamline, respectively. Figures 17 and 18 show the temperature contours for the augmented Burnett and the BGK–Burnett equations.

Conclusions

The two-dimensional augmented Burnett equations and the BGK–Burnett equations have been applied to compute the hypersonic blunt-body flow (for air) at Kn = 0.1, 0.01, and 0.001. The explicit finite difference scheme with Steger–Warming flux-vector splitting has been employed to discretize the convective terms in the flow equations. Second-order central differencing is used to discretize the stress and heat-flux terms. The density and temperature changes along the stagnation streamline are compared for each set of equations. At Kn = 0.1, the resulting flow properties and the shock structure are consistent with the results reported by Zhong.[2] At low Knudsen number ($Kn \leq 0.01$), the Navier–Stokes solutions and the two Burnett solutions are identical.

References

[1]Fiscko, K. A., and Chapman, D. R., *Comparison of Burnett, Super-Burnett and Monte Carlo Solutions for Hypersonic Shock Structure*, Vol. 118, Progress in Aeronautics and Astronautics, AIAA, Washington, DC, 1989, pp. 374–395.

[2]Zhong, X., "Development and Computation of Continuum Higher Order Constitutive Relations for High-Altitude Hypersonic Flow," Ph.D. Dissertation, Stanford Univ., Stanford, CA, 1991.

[3]Welder, W. T., Chapman, D. R., and MacCormack, R. W., "Eval-

uation of Various Forms of the Burnett Equations,'' AIAA Paper 93-3094, July 1993.

[4]Comeaux, K. A., Chapman, D. R., and MacCormack, R. W., ''An Analysis of the Burnett Equations Based on the Second Law of Thermodynamics,'' AIAA Paper 95-0415, Jan. 1995.

[5]Balakrishnan, R., and Agarwal, R. K., ''Numerical Simulation of Bhatnagar-Gross-Krook-Burnett Equations for Hypersonic Flow,'' *Journal of Thermophysics and Heat Transfer*, Vol. 11, No. 3, 1997, pp. 391–399.

[6]Hoffmann, K. A., ''Transformation of the Equations of Fluid Motion,'' *Computational Fluid Dynamics for Engineers*, 1st ed., Engineering Education System, Austin, TX, 1989, pp. 306–369.

[7]Steger, J. L., and Warming, R. F., ''Flux Vector Splitting of the Inviscid Gas Dynamics Equations with Application to Finite-Difference Methods,'' *Journal of Computational Physics*, Vol. 40, No. 2, 1981, pp. 263–293.